MEAN FLOW CHARACTERISTICS FOR THE OBLIQUE IMPINGEMENT OF AN AXISYMMETRIC JET

J. F. Foss
Associate Professor
Department of Mechanical Engineering
and
Division of Engineering Research
MICHIGAN STATE UNIVERSITY

S. J. Kleis*
Assistant Professor
Department of Mechanical Engineering
University of Houston

* Formerly, Graduate Assictant
Division of Engineering Research
MICHIGAN STATE UNIVERSITY

ABSTRACT

The oblique impingement of an axisymmetric jet has been investigated. A summary of the data and the analytical interpretations of the dominant mechanisms which influence the flow are reported. The major characteristics of the shallow angle oblique jet impingement flow field are:

1) minimal dynamic spreading as revealed by the surface pressure field,
2) pronounced kinematic spreading as revealed by the jet flow velocity field,
3) a pronounced upstream shift of the stagnation point from the maximum pressure point,
4) the production of streamwise vorticity by the impingement process.

This research work was supported by the NASA Lewis Research Center, Grant NGR 23-004-068.

1. INTRODUCTION

The oblique impingement of an axisymmetric jet on a large plane surface was the subject flow for the investigation reported herein. Figure 1 presents a schematic representation of the flow field and defines the variables used for its description. The objectives of the study were to identify the characteristics of this flow field and to infer the dominant mechanisms responsible for them. The shallow angle ($0 < \alpha \lesssim 12$ degree) cases were of primary concern; however, several larger angles were investigated for purposes of comparison.

This study was motivated by the externally blown flap configuration for a STOL aircraft. Specifically, if the populsion jet interacts with the airfoil surface prior to its impingement upon the extended flap (for an underwing configuration), then the proper design of the gap, between the airfoil and flap, must account for the nature of the flow resulting from this interaction. In particular, a gap which allows the streamwise vorticity (created by the interaction) to be passed to the suction side of the flap will provide an enhanced boundary layer control effect for the flow over the flap. The application to the over-the-wing configuration is even more apparent. The geometric range of experimental interest, $0.5 < h/d \leq 2$, $0 \leq x/d \leq 5$, was suggested by this motivation problem. The incidence angle and jet-plate separations examined are listed in Table 1.

Previous literature references on the shallow angle, oblique jet impingement flow field have not provided for its extensive documentation.

A wind tunnel simulation study by Raney and his associates [1] was carried out at the British R.A.E. Farnborough to evaluate the effects of an underslung engine placed in rather close proximity to the support wing. The investigation evaluated a configuration for an airbus, and a straight wing (no flap) was used with jet-to-free stream velocity ratios between 1 and 2 ($1 \leq u_{jet}/u_s \leq 2$); that is, a condition simulating a high speed forward flight was investigated. The actual engine geometry was simulated and this flow source was mounted on an airfoil. The object data were the pressures on the upper and lower surfaces of the airfoil. An incidence angle (α) of four degrees was employed for the majority of the tests, and h/d values of 0.65 to 0.88 were investigated. For the geometries and flow conditions evaluated, the upper surface pressure distribution remained unchanges from the condition in which only an airfoil was present. However, the lower surface pressure distribution

showed a strong dependence on the spacing (h/d) and velocity (u_s/u_j) ratio. It should be noted that STOL applications will involve much greater velocity ratios and possibly different engine configurations than those tested. The principal contribution of the Raney, et. al. report to the present study is considered to be the possible inference of free stream velocity effects.

Alexander, Baron and Comings have reported an extensive series of tests involving free jet flows [2]. They propose that the analytical approach due to Reichardt provides an effective calculation scheme for transport phenomena. As one aspect of this general study, they have recorded a limited quantity of data for two, parallel, round jets. The data are recorded for the plane defined by the jet axes and the streamwise direction (except for a symmetry plane traverse at x/d = 30). The data are reported for $x/d \geq 10$ and for a jet separation of (approximately) 2.4d. With the observation that the center plane is a plane of symmetry, they indicated that the two-jet flow field will be similar to that with a wall at the plane of symmetry. Their data for the latter case also commence at x/d = 10 and are only for the above indicated planes. The data for the case using the physical plane show somewhat greater velocities near the plane than the completely free condition. This observation, not explained by the authors, may be due to the generation of streamwise vorticity as discussed in the results section of the present writing.

Axisymmetric jets which are parallel to the wall have been investigated by Kuchemann [3] and Naib [4]. The jets were displaced above the surface for the former study and exhausted at the plane of the surface for the latter. The substantive information from both of these is primarily associated with the flow at downstream locations beyond the domain of the present study.

More extensive data is available for the large angle jet impingement case.

Yakovlevskii and Krasheninnikov [5], in a study of a round jet impinging on a flat plate at large angles, have indicated that the lower portion of the jet shows some reversed flow at an angle of 30-35 degrees. Their pressure data and velocity data were mainly in support of their interest in the flow at a considerable distance from the impingement point and is too coarse to be of value to the present study. Donaldson and Snedecker [6]

provide documentation of nozzle height, mach number, and large angle (α = 90, 60, 45, 35 degrees) effects on an impinging jet. Because of the reversed flow condition for angles larger than 30-35 degrees (an observation which they substantiate), the majority of their work does not overlap with or contribute directly to the present study. The pertinent features of their study are quoted along with the results presented herein. Westley, et. al. [7] present extensive data for surface pressure fluctuation intensities of normal and obliquely impinging jets ($22.5 \leq \alpha \leq 90$ degrees) for both super and subsonic mach numbers. Flow visualization by surface streaking markers is presented for a supersonic jet exit condition.

For completeness, it should be noted that there have been numerous studies of the vertical impingement of a round jet on a flat plate. Tani and Komatsu [8], Chao and Sandborn [9], and Poreh, et. al. [10] have recorded mean and turbulence quantities for such flows. A recent literature evaluation and further experimental results have been reported by Hrycak, et. al. [11]. Such flows are sufficiently different from the oblique impingement flow that they provide little assistance in the interpretation of the present results.

The three-dimensional field of a wall jet whose width/height ratio is near unity provides an instructive reference case for certain aspects of the subject problem. Extensive documentation of such a wall jet is provided by Sforza and Herbst [12].

The Experimental Faculity

The flow system was designed such that the jet could be formed from two different exit plane conditions; specifically, a fully developed pipe flow and a relatively short nozzle with a rather uniform mean velocity profile were used. The flow system is shown in Figure 2. The high pressure air for the jet was produced by means of a multiple stage centrifugal blower and was ducted through a counterflow heat exchanger in order to maintain the jet exit temperature at the ambient value. The blower and heat exchanger were placed in a separate room in order to ensure constant ambient conditions near the test facility during the course of a run. A plenum chamber was used to remove the large scale fluctuations from the flow. The fully developed pipe exit condition was obtained by a 3.66 m (12 ft.) long, 5.08 cm. (2 in.). I.D. extruded aluminum pipe giving exit velocities of about 37 mps (120 ft./sec.)

The pipe was supported such that h/d values between 0 and 2 could be obtained.

The flow system for the "uniform" exit profile consisted of a 15.2 cm (6 in.) I.D. extension of the plenum chamber terminated by a short radius contraction to a 30.5 cm. (12 in.) pipe. See Figure 3 for the detail of the nozzle and the exit plane velocity data. This configuration provided a compromise between a uniform exit condition and a geometry which minimized blockage effects (i.e., for entrainment) and allowed small values of h/d and α to be physically obtained.

A large plate, hinged to provide variable angles α, served as the plane-wall. A portion of the plate was movable, $\Delta y = \pm 5.08$ cm ($\pm$ 2 in.) and was driven in the y-direction by a computer controlled stepping motor. Two rows of surface static pressure taps, located at $y = \pm 5.08$ cm ($\pm$ 2 in.) were used for the static pressure data. The rows were staggered so that, if symmetry was assumed, a spacing as fine as .3175 cm (1/8 in.) in the x-direction could be obtained.

The movable plate section was also used to drive the hot-wire rake support head in the y-direction for the mean velocity traverses. The rake of four hot-wire probes was positioned in x and z and then traversed across in the y-direction at 0.254 cm (0.1 in.) intervals taking readings for 10 seconds at each point. This averaging time represents a compromise between the time required for a stationary signal in the outer region of the jet and the total time required for the quantity of data recorded. The acceptable data scatter in the velocity traverses justifies the selection of the averaging time. Disa, 55A22 hot-wires probes mounted in the x-y plane were used for the measurements. This probe has a known sensitivity to pitch effects, but no corrections to the data have been attempted since the objectives of the study were to provide data for an exploratory survey of the flow field.

The instrumentation and data acquisition system is shown in Figure 4. Within the constraints imposed by the hot-wire probe response, the normalized u/u_{max} data is quite accurate since calibration information for the four linearized wires was first stored in the computer and then used for the subsequent computation of the velocity and the position, and the record of the position, were under computer control.

Results and Discussion

Spreading and Curvature

The presence of the plate imposes a kinematic, no penetration, constraint on the behavior of the jet. The response of the jet fluid will be to spread horizontally and/or to deflect vertically with respect to the horizontal plate. The balance between these two effects is dictated by the dynamics of the interaction. The assessment of the relative spreading of the jet requires the definition of both an appropriate reference of the jet width in the absence of the plate and an appropriate measure of the deflected jet width. The former is provided by the intersection of the surface $u(x,r) = 0.1\, u_o$ and the plane of the plate. The experimental data in the free jet indicated that a cone, of half angle 5.7 degrees and 4 degrees for the fully developed and uniform cases respectively, quite adequately describes this surface for $0 \leq x/d \leq 5$. The intersection of the cone and the plane of the plate will form an ellipse, hyperbola or parabola depending upon the incidence angle of the cone.

The contours of constant pressure in the plane of the plate suggested an appropriate measure of the jet spread, see Figures 5 through 8. These figures, which include both the reference curve and the static pressure contours, indicate that there is little systematic spreading for the shallow angle ($0 < \alpha < 12$ degree cases). Data for the 15 and 30 degree conditions are included to demonstrate that this condition does not persist for the larger angles. The similarity between the shape of the reference curve and the shape of the isobars prompted a quantitative examination of their mutuality; the results of this survey are presented in Table 1. It can be seen that the reference curve width is approximately 70 percent that of the zero isobar contour and that a nominal value of 0.3 describes the isobar which aligns with this reference curve. (Note that there is a considerably greater variation in the set of values which forms the second of these two measures.) Table 1 also demonstrates the complete range of cases which were investigated; the complete results are available in the report by Foss and Kleis [13]. The static pressure contours serve to define what might be termed the "dynamic" jet width. Alternatively, the velocity field data constitutes the basis for a "kinematic" jet width. Isotach contours of the velocity field are shown for three characteristic cases in Figures 9 through 11. The lateral pressure distributions at the

same longitudinal locations, which are included as reference width measures, clearly show that the kinematic width increases much more rapidly with increasing angle than the dynamic width. The isotach contours which correspond with the zero pressure location, namely, $u/u_o = 0.1$, 0.3 and 0.5 for $\alpha = 3$, 9, and 15 degrees respectively, demonstrate this.

It is possible to rather accurately define the curvature of the jet from the extant experimental data. Specifically, the curvature K can be expressed as

$$K = [d^2 z_m/dx^2] [1 + (dz_m/dx)^2]^{-3/2} \tag{1}$$

where z_m is the vertical location of the jets momentum flux vector. The integral moment-of-momentum equation applied to a control volume which extends from the jet exit to an arbitrary downstream location and from the plate to the entrained flow region can be used to relate z_m to measurable quantities. Neglecting the second order momentum flux terms of the entrainment flow, this relationship is

$$\frac{z_m}{d} = \frac{h}{d} + \frac{x}{d}\frac{F_p}{J(o)\cos\alpha} - \frac{x}{d}\tan\alpha - \frac{1}{J(o)\cos\alpha}\int_{A_p}\frac{x}{d}\,p\,dA \tag{2}$$

which also implicitly considers the x-component momentum flux to be a constant.* Using this expression for z_m, the curvature K can be evaluated as

$$K = \frac{\frac{1}{J(o)\cos\alpha}\int_{-\infty}^{\infty} p\,dy}{\left[\left(\frac{F_p}{J(o)\cos\alpha} - \tan\alpha\right)^2 + 1\right]^{3/2}} \tag{3}$$

and considering that the denominator of (3) is not significantly different from unity** for the shallow angle cases, the further condition that

$$\int_o^{\infty} K\,dx \cong \tan\alpha \tag{4}$$

may be established as an integral reference condition for the K(x) curves.

* This assumption is equivalent to neglecting the shear force on the plate from 0→x. A separate experiment showed that the maximum shear force was less than 2 percent of J(o).

** Note that $0 \le F_p/J(o)\cos\alpha \le \tan\alpha$ and $\tan^2\alpha < 0.072$ for $\alpha \le 15$ degrees.

Sample K(x) curves are presented in Figure 12. Unlike the jet width characteristics, no simple measures of the curvature were suggested by the data and no simple trends in the K(x) curves, as a function of α and h/d, were observed. Based upon the approximate relationship (4) and the area under the K(x) curves, it is apparent that the jets will continue to curve for a considerable distance downstream of the measurement region.

Stagnation Phenomena

On a gross scale, the jet flow impacts upon the plate, deflects vertically and/or spreads laterally as noted above. More precisely, only the stagnation streamline* impacts upon the plate; it is the purpose of this section to examine the nature of the stagnation phenomena both analytically and experimentally. Analytically, the relationship between the streamline orientation at the plate surface and the surface pressure and vorticity gradients will be established. Experimentally, the location of the stagnation point will be inferred.

The analysis which relates the orientation of the stagnation streamline to the characteristics of the flow is presented in the Appendix. The terms used in the analysis are identified in Figure 13 and the final result, viz,

$$\xi'(0) = - \frac{3\mu(\partial \omega_y/\partial x)_{z=0}}{\partial p/\partial x} \qquad (5)$$

can be used to infer that the stagnation point can be location in a region of adverse pressure gradient or at a pressure maxima. That is, since $0 > \xi'(0) \geq -\infty$ (based upon the geometric shape of the stagnation stremline), and since $(\partial \omega_y/\partial x) > 0$ (based upon the condition that the flow is directed away from the point x_s, it is necessary that $\partial p/\partial x \geq 0$ such that the r.h.s. of (5) is negative. The condition that $\partial p/\partial x = 0$ describes the vertical impingement case.

*Time averaged quantities are exclusively considered in this section. The stagnation streamline is defined as the locus of points everywhere tangent to the velocity field with a terminus (the stagnation point) on the impact plate. The presence of a finite length stagnation line will be suggested by the experimental data and it cannot be excluded by analytical considerations. However, the general discussion and the analysis will implicitly assume a single stagnation streamline.

The experimental technique to identify the stagnation point is based upon the equivalence of the stagnation pressure at z = 0 and a small δz value above the plate; i.e., δz is assumed small enough that the alteration of the stagnation pressure resulting from shear effects is negligible. The technique also assumes that the δz value is sufficiently large such that the static pressure is essentially equal to the atmospheric value. A schematic representation of the measurement technique is presented in Figure 13. For convenience of representation, the surface static pressures were converted to an equivalent "stagnation streamline" velocity v_p; that is

$$v_p(x) = \{2[\, p(x,0,0) - p_{atm}]/\rho \}^{1/2} \tag{6}$$

A Disa gold plated probe (to reduce pitch effects) was traversed at y = 0 and z = δz and the velocity v_w was recorded and transferred to the location of the plate along a ray which accounted for the inclination angle (α) and the divergence angle of the 0.1 isotach (β); viz, $v_w(x, \delta z)$ was shifted by an amount δx where

$$\delta x = \delta z \tan^{-1} (\alpha + \beta). \tag{7}$$

The stagnation point is considered to be the point of tangency between the $v_w(x)$ and $v_p(x)$ curves. In general, δz was sufficiently small ($\delta z/d \simeq 0.04$) that the first assumption was reasonably well satisfied. If the static pressure at (x, δz) exceeded the atmospheric value then the true stagnation point would lie farther upstream than that indicated.

The experimental data for α = 3, 9, and 15 degrees are presented in Figures 14 through 16. Considering that a stagnation point necessarily exists, the v_w curve was shifted farther downstream for the α = 3 degree case; apparently, the downstream pressure on the plate structurally deflects the low velocity fluid of the approaching jet. An opposite sense shift was introduced for the α = 15 degree data since the surface pressure cannot exceed the equivalent stagnation streamline value. Alternatively, this could logically be considered to indicate a violation of the "atmospheric pressure at δz" assumption. Significantly, the indicated stagnation points: $x_s/d \simeq 3.8$, 1.9, 1.3 for the conditions: uniform nozzle, h/d = 1 and α = 3, 9, 15 degrees respectively, are close to the intersections of the 0.1 isotachs with the plane of the plate. As noted earlier, the overlapping $v_w(x)$ and

$v_p(x)$ curves suggest the possibility of a finite length stagnation line (i.e., the curves appear to be tangent over a region). Excluding this, the orientation of the streamline at the stagnation point could be interpretted by equation 10 if the x gradient of ω_y were available.

Jet Flow Characteristics

The isotach contours of Figures 9 through 11, which are characteristic of those reported by Foss and Kleis [13], demonstrate the effect of the interaction on the jet. A striking feature of these curves is the preservation of the axisymmetric structure for the portion of the jet removed from the plate. For the shallow angle cases (i.e., α = 3 and 9 shown herein) the axisymmetric region is joined to the "near wall" region by a "buffer" region. The near wall region is characterized by tightly spaced isotachs which are parallel to the plate and transverse to the jet flow axis. The buffer region, which joins the axisymmetric portion to the near wall region, is characterized by the skirts of the jet which spread laterally outward near the plate surface. If the jet approach toward the plate is sufficiently rapid, then the upper axisymmetric portion is not preserved; see, for example, the results for α = 15 degrees, h/d = 1.

A significant characteristic of the jet flow is implied, but not revealed explicitly, by the isotach patterns. Specifically, the lateral edges of the jet suggest the presence of streamwise vorticity near the plate ($\mp \omega_x$ for $\mp$ y respectively). This vorticity is created by the surface pressure field and the "vortex-stretching" effects within the jet flow itself. These source effects are revealed by the control volume form of the vorticity transport equation*.

* This equation can be readily derived by forming the curl of the Navier-Stokes equations, forming its volume integral, using the Gauss Theorem to replace volume with surface integrals and utilizing the Navier-Stokes equations to replace the terms involving the viscosity and vorticity gradients with the surface pressure gradient terms. Specifically, for the latter,

$$\int_{c.s.} \nu\left(\frac{\partial}{\partial x_j}\omega_i\right) n_j \, dA \cong \int_{A_p} \left[\hat{i}\,\nu\frac{\partial}{\partial z}\left(\frac{\partial v}{\partial z}\right) - \hat{j}\,\nu\frac{\partial}{\partial z}\left(\frac{\partial u}{\partial z}\right) - \hat{k}\,\frac{\partial}{\partial z}\omega_z\right] dA$$

$$= \int_{A_p} \left[\hat{i}\,\frac{1}{\rho}\frac{\partial p}{\partial y} - \hat{j}\,\frac{1}{\rho}\frac{\partial p}{\partial x} \hat{k}\,\frac{\partial}{\partial z}\omega_z\right] dA$$

Where the approximation is for the replacement of the integral over the control surface with the integral over the impact plate (A_p). Note that the other substitutions are exact.

$$\int_{c.s.} \overline{\vec{\omega}\,(\vec{u}\cdot\hat{n})}\,dA = \int_{c.v.} \overline{\vec{\omega}\cdot\nabla\vec{u}}\,dv + \hat{i}\int_{A_p}\frac{1}{\rho}\,\frac{\partial p}{\partial y}\,dA$$

$$-\hat{j}\int_{A_p}\frac{1}{\rho}\,\frac{\partial p}{\partial x} - \hat{k}\int_{A_p}\frac{\partial \omega_z}{\partial z}\,dA \qquad (8)$$

For the application of this equation to the oblique jet impingement flow, consider a control volume bounded by the downstream plane of interest, (e.g., $0 \le y \le y_e$ and $0 \le z \le z_e$ where y_e and z_e are sufficiently large that they are in the entrainment region), the $y = 0$ and $z = 0$ planes and an upstream face across the approach jet. A small influx of positive x-component vorticity will result from the x projection of the azimuthal vorticity of the approach flow. A large efflux of negative ω_x can be expected as a result of the $(\partial p/\partial y)$ term, see Figures 5 through 8, and as a result of the production term $(\vec{\omega}\cdot\nabla\vec{u})$. Specifically, the vorticity in the y-z plane, which is parallel to the isotachs shown in Figures 9 through 11, will be strained into the x-direction by the $\partial u/\partial z$ and $\partial u/\partial y$ velocity gradients. Qualitative observations of ω_x with a crossed vane "vorticity meter" confirmed this interpretation of the control volume equation; no quantitative measurements were attempted. These characteristics of the isotach patterns are also revealed by the three-dimensional wall jet data of Sforza and Herbst [12]. However, the rectangular geometry of the wall jet suggests that its isotach pattern is the result of the vortex filament reorientation as observed in the related flows of Viets and Sforza [16] and Holdeman and Foss [17].

Summary and Conclusions

For a sufficiently gradual approach toward the plate, the dynamic width of the impinging jet as revealed by the surface pressure field, is not significantly larger than the undeflected jet. The kinematic jet width, as revealed by the velocity field measurements near the plate, does increase monotonically as the rate of approach is increased. (The rate of approach is increased as the angle, α, is increased and/or as the position of the jet above the plate, h, is decreased.)

The orientation of the stagnation streamline at the plate surface is analytically related to the pressure gradient and the x gradient of the transverse vorticity. The possible location of the stagnation streamline in an adverse or zero pressure gradient is established analytically and

experimental data, which show it to be located in the adverse pressure gradient region substantially upstream of the maximum pressure location, are presented.

The inference of strong streamwise vorticity production is established based upon a control volume description of the vorticity transport equation and the experimental data.

References

[1] D. J. Raney, A. G. Kurn and J. A. Bagley, "Wind Tunnel Investigation of Jet Interference for Underwing Installation of High By-pass Ratio Engines," ARC-CP-1044 (RAE, Farnborough, 1961). STAR Code N69 38230.

[2] L. G. Alexander, T. Baron and E. W. Comings, "Transport of Momentum, Mass and Heat in Turbulent Jets," University of Illinois, Engineering Experiment Station, Bulletin 413, (1953), pp. 7-88.

[3] Kuchemann, D., "Jet Diffusion in Proximity of Wall," NASA TM 1214 (1949).

[4] Naib, S.K.A., "Spreading and Development of the Parallel Wall Jet," Aircraft Engineering, Vol. 40, Dec. 1968, pp. 30-33.

[5] Yakovlevskii, O. V. and S. Y. Krasheninnikov, "Spreading of a Turbulent Jet Impinging on a Flat Surface," Fluid Dynamics 1, 4, (July-August 1966), pp 136-139.

[6] Donaldson, C. DuP. and R. S. Snedecker, "A Study of Free Jet Impingement, Part 1, Mean Properties of Free and Impinging Jets," J. Fluid Mech. 45, (1971), pp 281-319.

[7] Westley, R., J. H. Wooley and P. Brosseau, "Surface Pressure Fluctuations from Jet Impingement on an Inclined Flat Plate," AGARD Conference No. 113, Symposium on Acoustic Fatigue, May 1973, pp. 4-1 to 4-17.

[8] Tani, I. and Y. Komatsu, "Impingement of a Round Jet on a Flat Surface," Proc. 11th Int. Cong. Appl. Mech., 1964, H. Goertler, Ed., Springer Verlag, pp 672-676 (1966).

[9] Chao, J. L. and V. A. Sandborn, "Evaluation of the Momentum Equation for a Turbulent Wall Jet," J. Fluid Mech. 26, (1966) pp 819-828.

[10] Poreh, M., Y. G. Tsuei and J. E. Grmak, "Investigation of a Turbulent Radial Wall Jet," Jour. App. Mech. 34, No. 2, 1967, pp 457-463.

[11] Hrycak, P., D. T. Lee and J. W. Gauntner, "Experimental Flow Characteristics of a Single Turbulent Jet Impinging on a Flat Plate," NASA TN D-5690, March 1970.

[12] Sforza, P. M. and G. Herbst, "A Study of Three-Dimensional, Incompressible, Turbulent Wall Jets," AIAA Journal, 8, No. 2, February 1970, pp 276-283.

[13] Foss, J. F. and S. J. Kleis, "A Study of the Round-Jet/Plane-Wall Flow Field," First Annual Report, Grant NGR 23-004-068, Michigan State University, October 8, 1971.

[14] Lighthill, M. H., "II. Introduction. Boundary Layer Theory," Chapter 1 of Part II of Laminar Boundary Layers, L. Rosenhead, Ed., Oxford University Press, 1963, pp 46-60.

[15] Oswatitsch, K., "Die Ablosungsbedingung von Grenzschichtiten," Boundary Layer Research, Ed. H. Goertler, IUTAM Symposium Freiburg/BR. 1957, Springer-Verlag Berlin, 1958, pp357-367.

[16] Viets, H. and P. M. Sforza, "Dynamics of Bilaterally Symmetric Vortex Rings," Physics of Fluids, 15, No. 2, February 1972, pp 230-240.

[17] Holdeman, J. D. and J. F. Foss, "The Initiation, Development and Decay of the Secondary Flow in a Bounded Jet," ASME Paper No. 73-WA/Flcs-7. To be published in Jour. Fluids Engr. ASME.

Appendix*

The relationship between the flow field characteristics and the orientation of the stagnation streamline at the stagnation point is derived below. The analysis was stimulated by the observation that the measured stagnation point was located in the adverse pressure gradient upstream of the maximum pressure. The basic considerations employed in this analysis were largely abstracted from the Lighthill presentation of the vorticity equations, see Rosenhead [14]. Similar analytical developments are presented by Oswatitsch [15].

Using the symbols introduced in Figure 13, the orientation of the stagnation streamline can be expressed as $[dZ/dX]_{\beta = 0}$ where $Z = Z(\beta)$, $X = X(\beta)$ and β is the arc length measured upstream along the stagnation streamline. The components of the velocity vector in the neighborhood of $\beta = 0$ can also be used to describe the orientation of the streamline; viz.,

$$\lim_{\beta \to 0} \frac{w(\beta)}{u(\beta)} = \frac{dZ}{dX} \Big]_{\beta = 0} \tag{A.1}$$

Taylor series expansions for $w(\beta)$ and $u(\beta)$ can be used to describe the l.h.s. of (A.1). Specifically,

$$\begin{aligned} w(\beta) &= w(0) + w'(0)\beta + w''(0)\frac{\beta^2}{2!} + \ldots \\ u(\beta) &= u(0) + u'(0)\beta + u''(0)\frac{\beta^2}{2!} + \ldots \end{aligned} \tag{A.2}$$

The derivatives in A.2 can be expressed in terms of the velocity field derivatives in the cartesian coordinates (x, y) as, for example,

$$w'(\beta) = \frac{\partial w}{\partial x} X'(\beta) + \frac{\partial w}{\partial z} Z'(\beta) \tag{A.3}$$

and

$$w''(\beta) = \frac{\partial^2 w}{\partial x^2} [X'(\beta)]^2 + 2\frac{\partial^2 w}{\partial x \partial z} [X'(\beta)\, Z'(\beta)] + \frac{\partial^2 w}{\partial z^2} [Z'(\beta)]^2 + \frac{\partial w}{\partial x} [X''(\beta)] + \frac{\partial w}{\partial z} [Z''(\beta)] \tag{A.4}$$

The substition of these relationships into (A.2) (for the purpose of forming the ratio required for (A.1) can be substantially simplified

*The authors gratefully acknowledge the assistance of Prof. D. Yen, M.S.U., Dept. of Mathematics, for the development of the equations in this analysis.

by noting the terms which are equal to zero. Specifically,

$$w(0) = u(0) = \frac{\partial w}{\partial x}(0) = \frac{\partial w}{\partial z}(0) = \frac{\partial u}{\partial x}(0) = \frac{\partial^2 w}{\partial x \partial z}(0) = 0$$

Hence

$$\left.\frac{dZ}{dX}\right]_{\beta = 0} = \lim_{\beta \to 0} \frac{w''(0)\,\beta^2/2 + 0(\beta^3)}{u'(0)\,\beta + u''(0)\,\beta^2/2 + 0(\beta^3)}$$

$$= \lim_{\beta \to 0} \frac{\frac{\partial^2 w}{\partial z^2}(0)\,[Z'(0)]^2\,(\beta^2/2)}{\frac{\partial u}{\partial z}(0)\,\beta + \{2\frac{\partial^2 u}{\partial x \partial z}(0)\,[X'(0)\,Z'(0)] + \frac{\partial^2 u}{\partial z^2}(0)\,[Z'(0)]^2\}(\beta^2/2)} \qquad \text{(A.5)}$$

The l.h.s. of (A.5) is non-zero; hence, $\partial u/\partial z(0)$ must be zero for otherwise the r.h.s. of (A.5) would approach zero in the limit as $\beta \to 0$. The ratio of the $Z'(0)$ and $X'(0)$ values is equal to the desired slope, that is,

$$\frac{Z'(0)}{X'(0)} = \frac{dZ}{d\beta}(0)\,\frac{d\beta}{dX}(0) = \frac{dZ}{dX}(0)\,. \qquad \text{(A.6)}$$

Dividing the non-zero terms of (A.5) by $[X'(0)\;\; Z'(0)]\,(\partial^2 w/\partial z^2)(\beta^2/2)$ yields the expression

$$\frac{dZ}{dX}(0) = \frac{\frac{Z'(0)}{X'(0)}}{2\frac{\frac{\partial^2 u}{\partial x \partial z}}{\frac{\partial^2 w}{\partial z^2}} + \frac{\frac{\partial^2 u}{\partial z^2}}{\frac{\partial^2 w}{\partial z^2}}\,\frac{Z'(0)}{X'(0)}} \qquad \text{(A.7)}$$

Forming the z partial derivative of the conservation of mass expression, $\partial(\nabla \cdot \vec{V})/\partial z = 0$, evaluated at the symmetry plane where $\partial v/\partial y = 0$, yields the equality

$$-\frac{\partial^2 u}{\partial x \partial z} = \frac{\partial^2 w}{\partial z^2} \qquad \text{(A.8)}$$

Substituting (A.8) into (A.7) and noting that the denominator must be equal to 1, results in the following expressions for the slope of the stagnation streamline

$$\frac{dZ}{dX}(0) = \frac{2\dfrac{\partial^2 w}{\partial z^2}}{\dfrac{\partial^2 u}{\partial z^2}} \qquad (A.9)$$

$$= \frac{-3\mu\{\partial \omega_y/\partial x}{\partial p/\partial x}$$

Table 1. Summary of percent widths, distance to maximum pressure and isobar which aligns with free isotach intersection.

		Width of 0.1 free isotach intersection contour as a percentage of the zero isobar width recorded at the x-location of the maximum pressure		x/d distance from x=o to p max		p_{agree_2} $\lambda \rho u(0)^2 \sin \alpha$ all x 10^{-2}		x/d distance from x=0 to 0.1 free isotach intersection	
α	h/d	u	fd	u	fd	u	fd	u	fd
3	0.5625	--	74	--	0.7	--	0.57	--	0.321
	0.667	--	80	--	2.3	--	0.31	--	1.003
	0.75	0.75	80	4.5	2.9	0.35	0.266	1.663	1.544
	1	0.68	78	5.9	5.7	0.38	0.266	3.543	3.176
6	0.75	0.69	76	1.9	2.1	0.36	0.30	1.16	1.18
	1	0.75	71	4.7	4.2	0.29	0.30	2.5	2.324
	1.5	0.64	68	6.4	7	0.20	0.22	5.178	4.737
9	1	0.64	71	3.2	3.3	0.38	0.27	1.91	1.81
	1.5	0.65	70	5.7	6.2	0.25	0.22	3.715	3.979
	2	--	66	--	7.5	--	0.18	--	5.619
12	1	--	--	--	--	--	--	--	--
	1.5	0.58	65	5	5.1	0.28	0.224	3.202	3.029
	2	--	65	--	7.2	--	0.22	--	4.59
15	1	0.46	--	2	--	1.0	--	1.247	--
	1.5	--	--	--	--	--	--	--	--
	2	--	61	--	6	--	0.24	4.06	3.855
30	2	0.3	--	3.4	--	0.65	--	1.978	--
	3	0.36	--	5.2	--	0.61	--	3.429	--
60	2	0.25	--	1.9	--	0.92	--	0.37	--

Figure Captions

Figure 1 The Coordinate System and a Schematic representation of jet impingement flow field

Figure 2 The jet impingement flow system

Figure 3 The "uniform flow" nozzle geometry and the exit plane velocity distribution

Figure 4 The data acquisition system

Figure 5 Surface isobars for the conditions α = 3 degrees, h/d = 1, uniform nozzle Note: numerical values represent $[p(x, y, 0)/ p\lambda u(0)^2 \sin \alpha] \times 10^2$ where λ = momentum flux correction factor = 0.809 and u(0) = velocity at the jet exit centerline = 120 fps; $u(0)\, d/\nu \approx 10^5$

Figure 6 Surface isobars for the conditions α = 9 degrees, h/d = 1, uniform nozzle (Contour numerical values defined in Figure 5).

Figure 7 Surface isobars for the conditions α = 15 degrees, h/d = 1, uniform nozzle (Contour numerical values defined in Figure 5).

Figure 8 Surface isobars for the conditions α = 30 degrees, h/d = 1, uniform nozzle (Contour numerical values defined in Figure 5).

Figure 9 Isotach contours for the conditions α = 3 degrees, h/d = 1, uniform nozzle. (Contour numerical values represent u/u_{max} at the indicated x/d location)

Figure 10 Isotach contours for the conditions α = 9 degrees, h/d = 1, uniform nozzle (Contour numerical values represent u/u_{max} at the indicated x/d location)

Figure 11 Isotach contours for the conditions α = 15 degrees, h/d = 1, uniform nozzle (Contour numerical values represent u/u_{max} at the indicated x/d location)

Figure 12 Curvature, K, of the approaching jet as a function of the incidence angle and initial elevation

Figure 13 Stagnation Point phenomena

a.) Definition of terms used in the stagnation point analysis

b.) Experimental technique to locate the stagnation point

Figure 14 Experimental evaluation of the stagnation point for the conditions, α = 3 degrees, h/d = 1, uniform nozzle
(Note, the stagnation "point" is inferred to be the point of tangency between the velocity measured by the hot-wire, v_w, and the velocity computed from the measured surface static pressure, v_p.)

Figure 15 Experimental evaluation of the stagnation point for the conditions α = 9 degrees, h/d = 1, uniform nozzle. (See Figure 14 for interpretation of data).

Figure 16 Experimental evaluation of the stagnation point for the conditions α = 15 degrees, h/d = 1, uniform nozzle.
(See Figure 14 for interpretation of data).

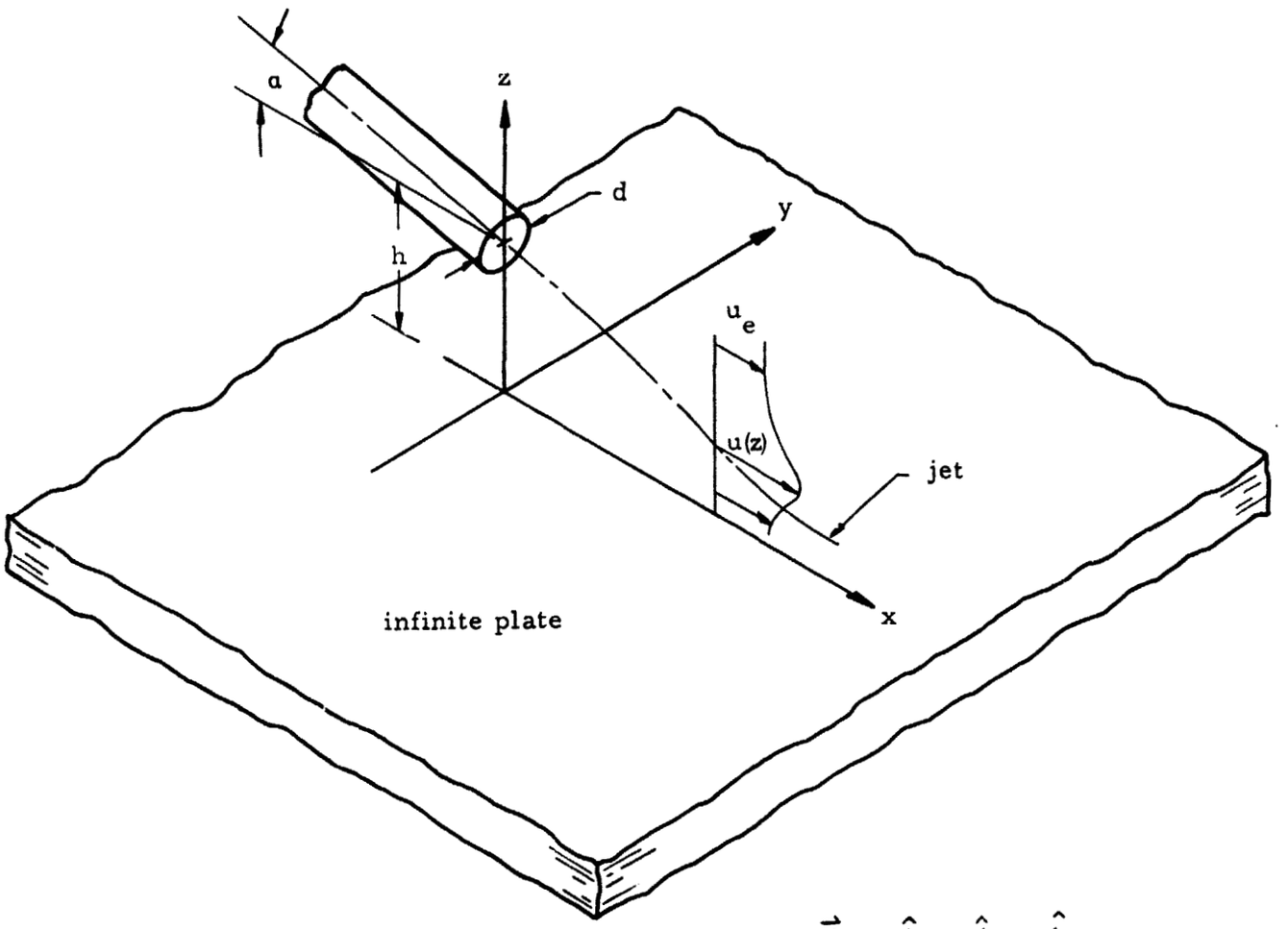

$$\vec{V} = \hat{i}\,u + \hat{j}\,v + \hat{k}\,w$$

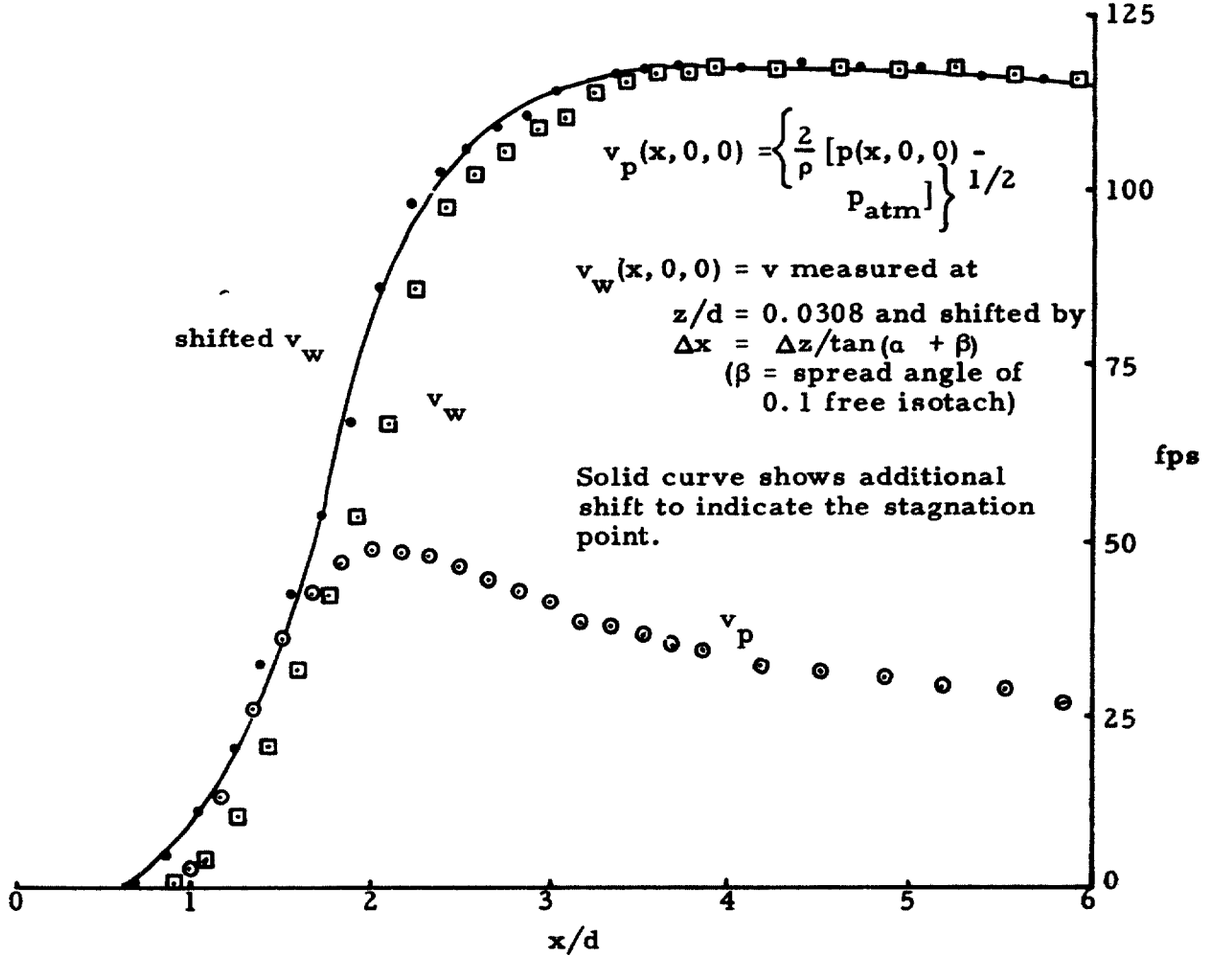
125
100
75
50
25
0
fps
0
1
2
3
4
5
6
x/d
$v_p(x,0,0) = \left\{\frac{2}{\rho}[p(x,0,0) - p_{atm}]\right\}^{1/2}$
$v_w(x,0,0)$ = v measured at z/d = 0.0308 and shifted by $\Delta x = \Delta z/\tan(\alpha + \beta)$ (β = spread angle of 0.1 free isotach)
Solid curve shows additional shift to indicate the stagnation point.
shifted v_w
v_w
v_p

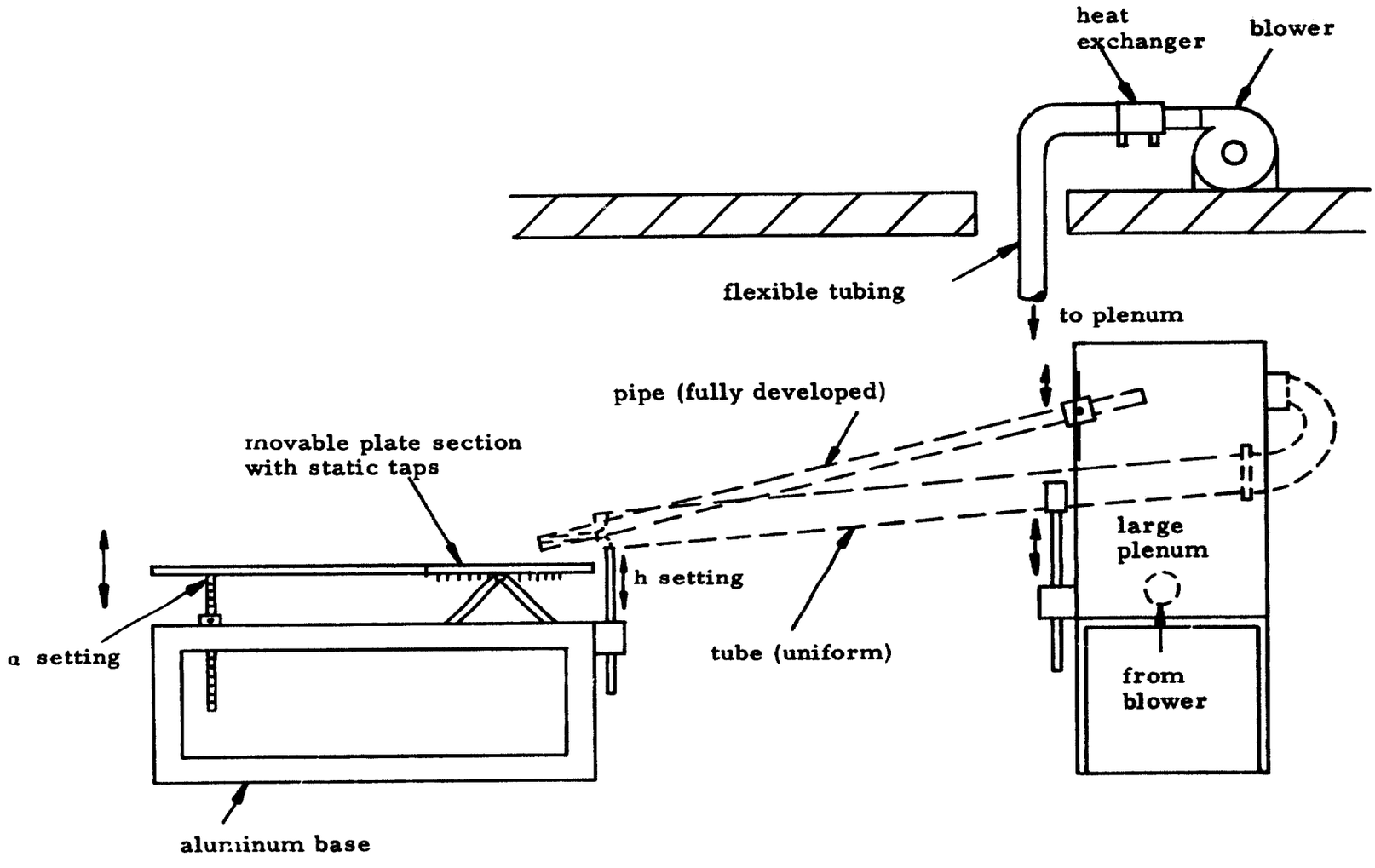
heat exchanger
blower
flexible tubing
to plenum
pipe (fully developed)
movable plate section with static taps
h setting
α setting
tube (uniform)
large plenum
from blower
aluminum base

r/r_o	0	0.05	0.10	0.15	0.20	0.25	0.30	0.35	0.40	0.45
u/u(0)	1	1	1	1	1	1	1	1	1	1
r/r_o	0.50	0.55	0.60	0.65	0.70	0.75	0.80	0.85	0.90	0.95
u/u(0)	1	1	0.99	0.98	0.96	0.93	0.90	0.83	0.72	0.52

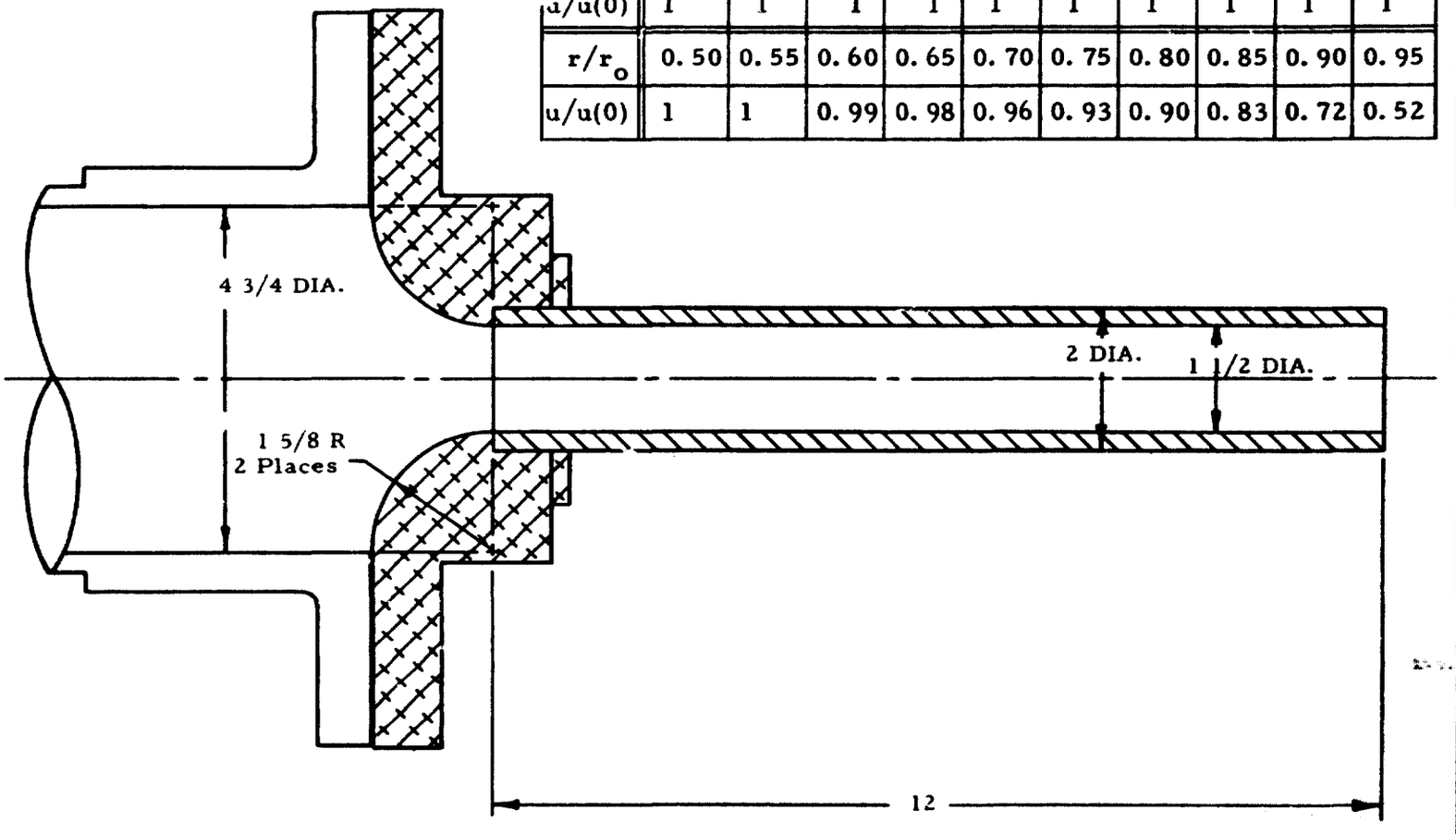

SCALE: HALF

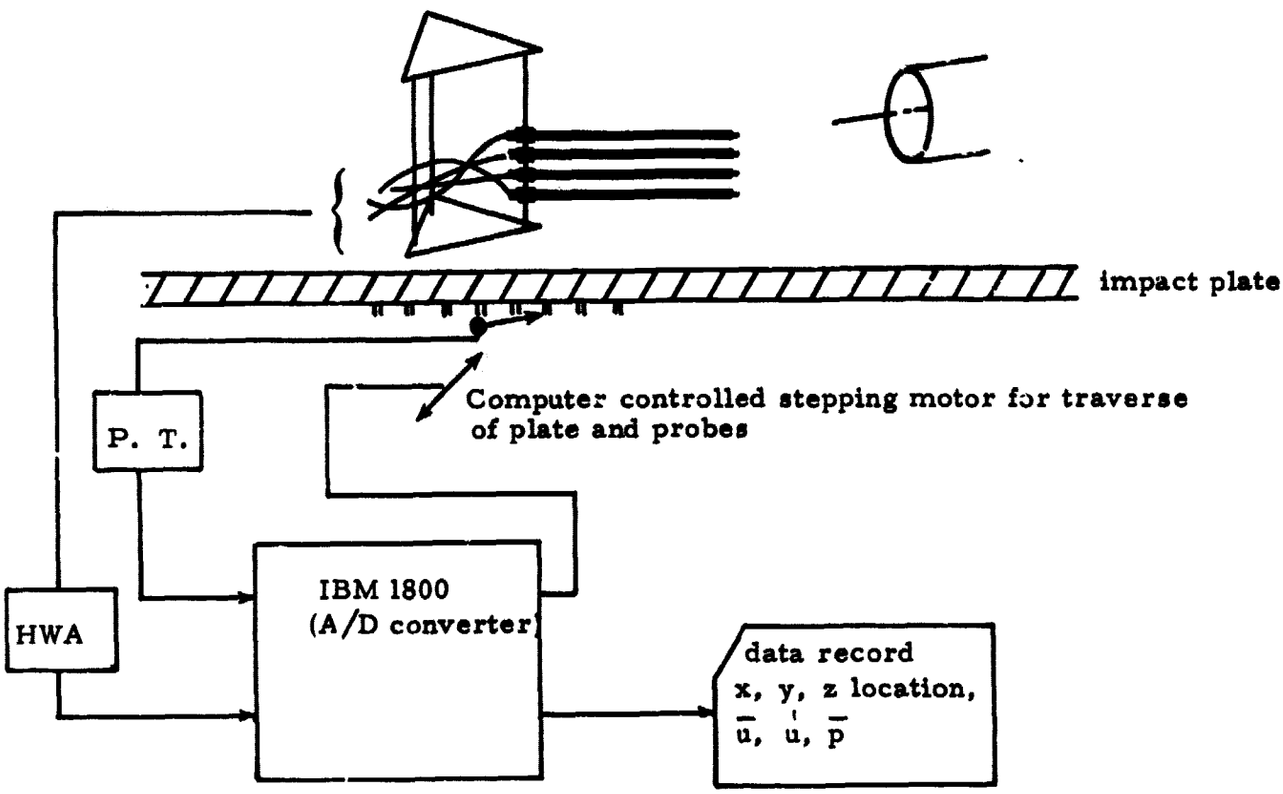

HWA hot-wire anemometer (2-T.S.I. 1054-A (linearized)
Disa 55 DO5 w/55D15 linearizer
Disa 55 AO1 w/ 55D15 linearizer

P. T. pressure transducer (Decker Model 308-3)

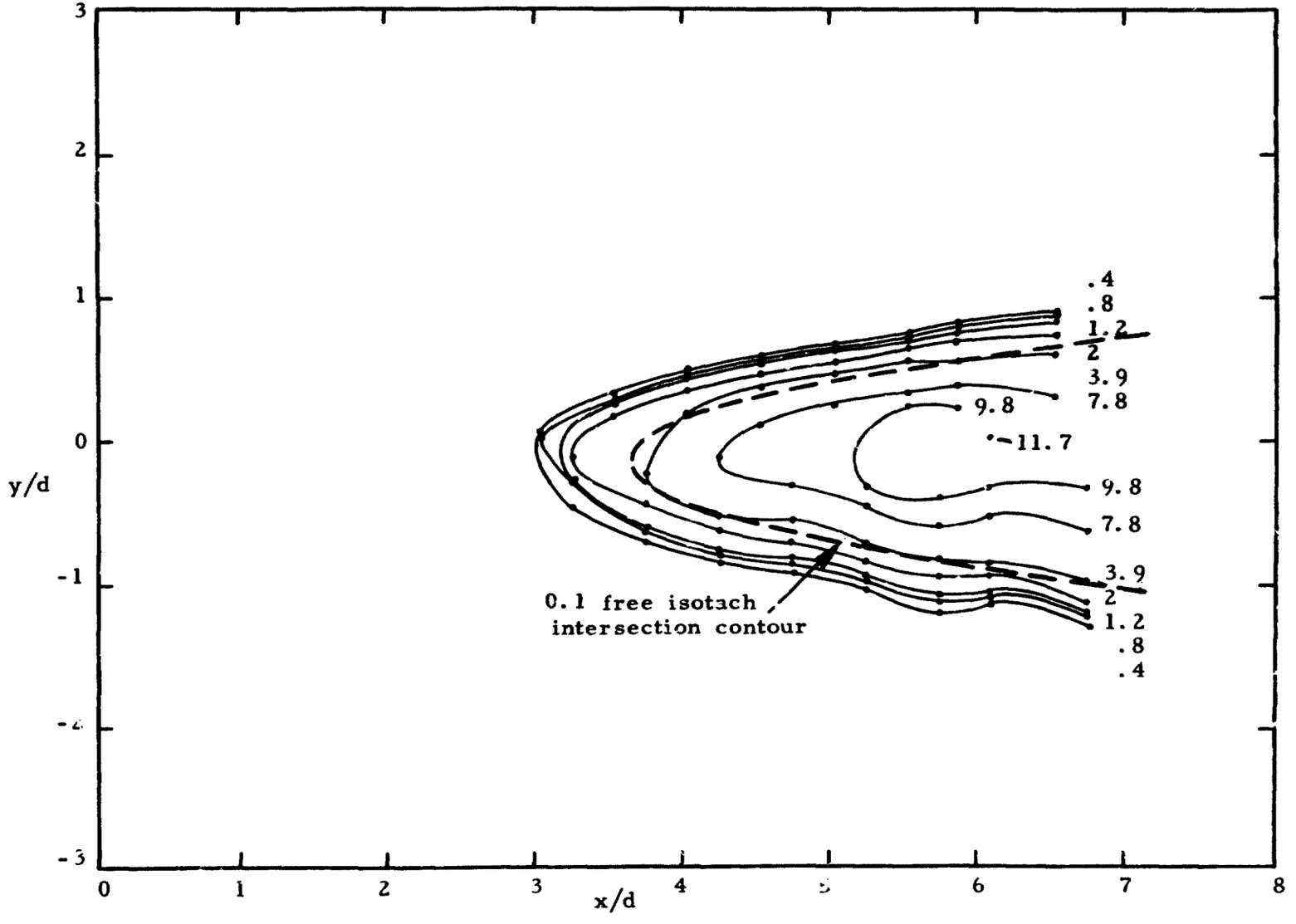
3
2
1
0
-1
-2
-3
y/d
0
1
2
3
4
5
6
7
8
x/d
.4
.8
1.2
2
3.9
7.8
9.8
11.7
9.8
7.8
3.9
2
1.2
.8
.4
0.1 free isotach
intersection contour

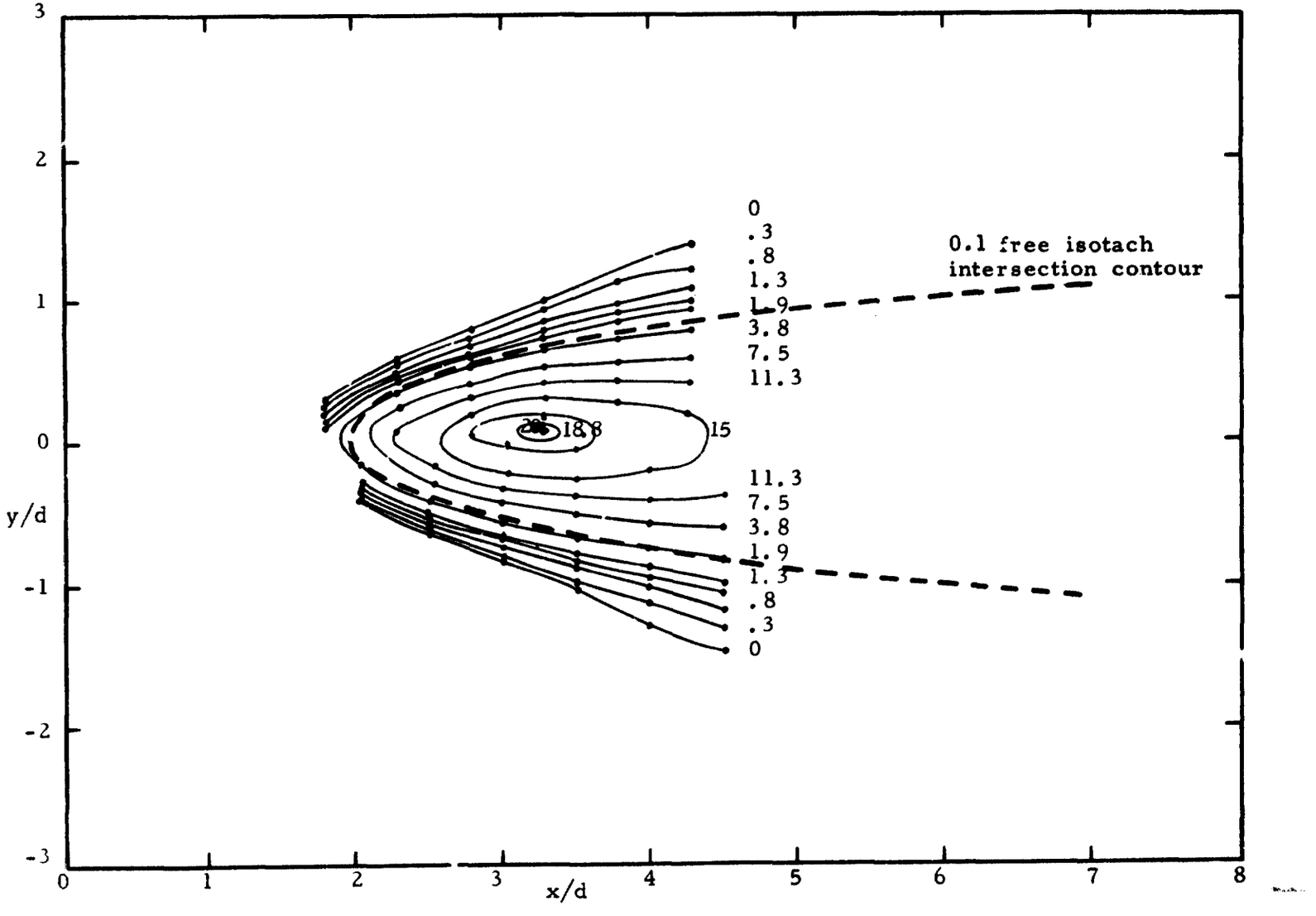
0
.3
.8
1.3
1.9
3.8
7.5
11.3
18.8
15
11.3
7.5
3.8
1.9
1.3
.8
.3
0
0.1 free isotach
intersection contour
y/d
x/d
3
2
1
0
-1
-2
-3
0
1
2
3
4
5
6
7
8

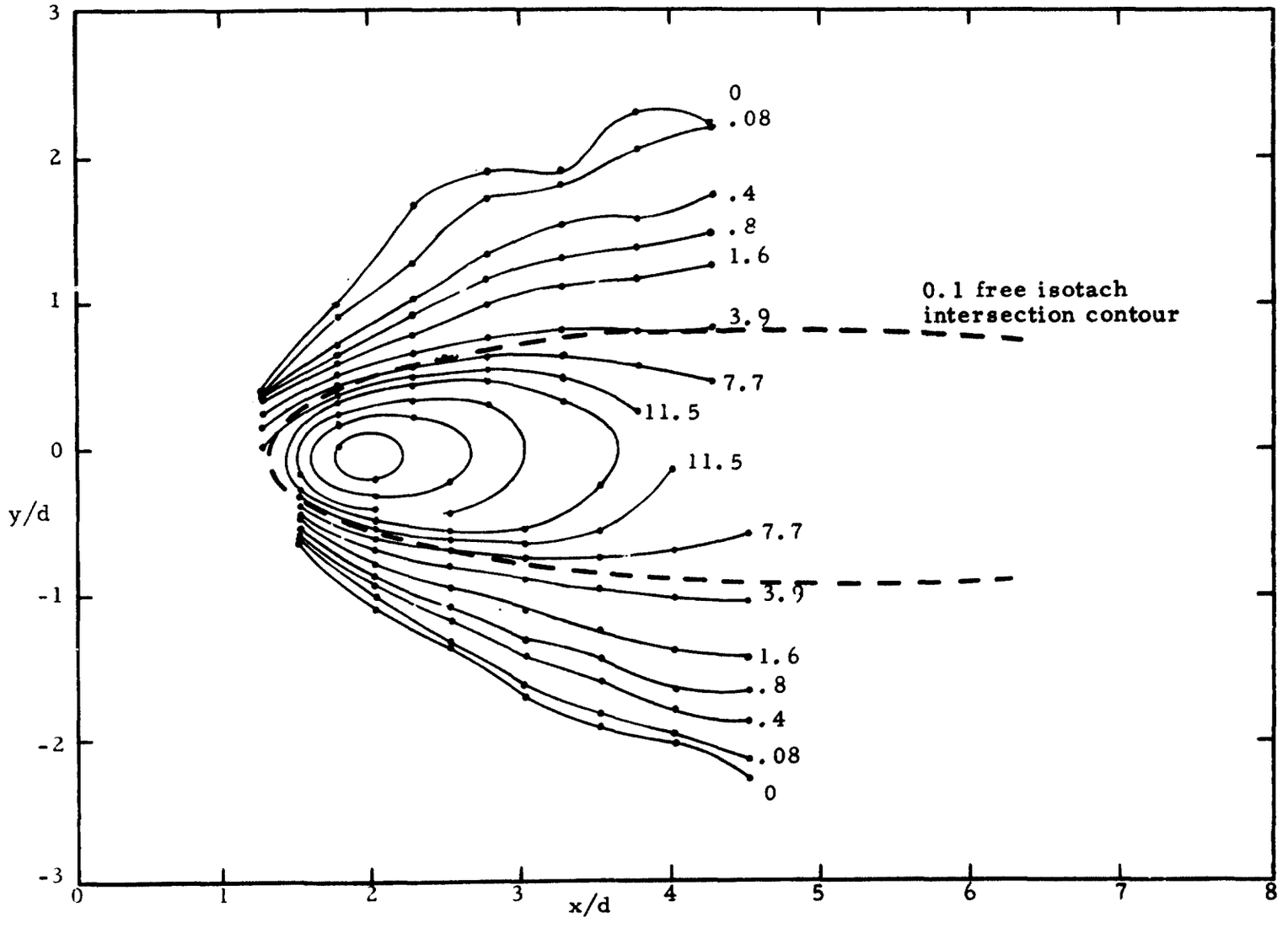
0
.08
.4
.8
1.6
3.9
7.7
11.5
11.5
7.7
3.9
1.6
.8
.4
.08
0
0.1 free isotach intersection contour
y/d
x/d
3
2
1
0
-1
-2
-3
0
1
2
3
4
5
6
7
8

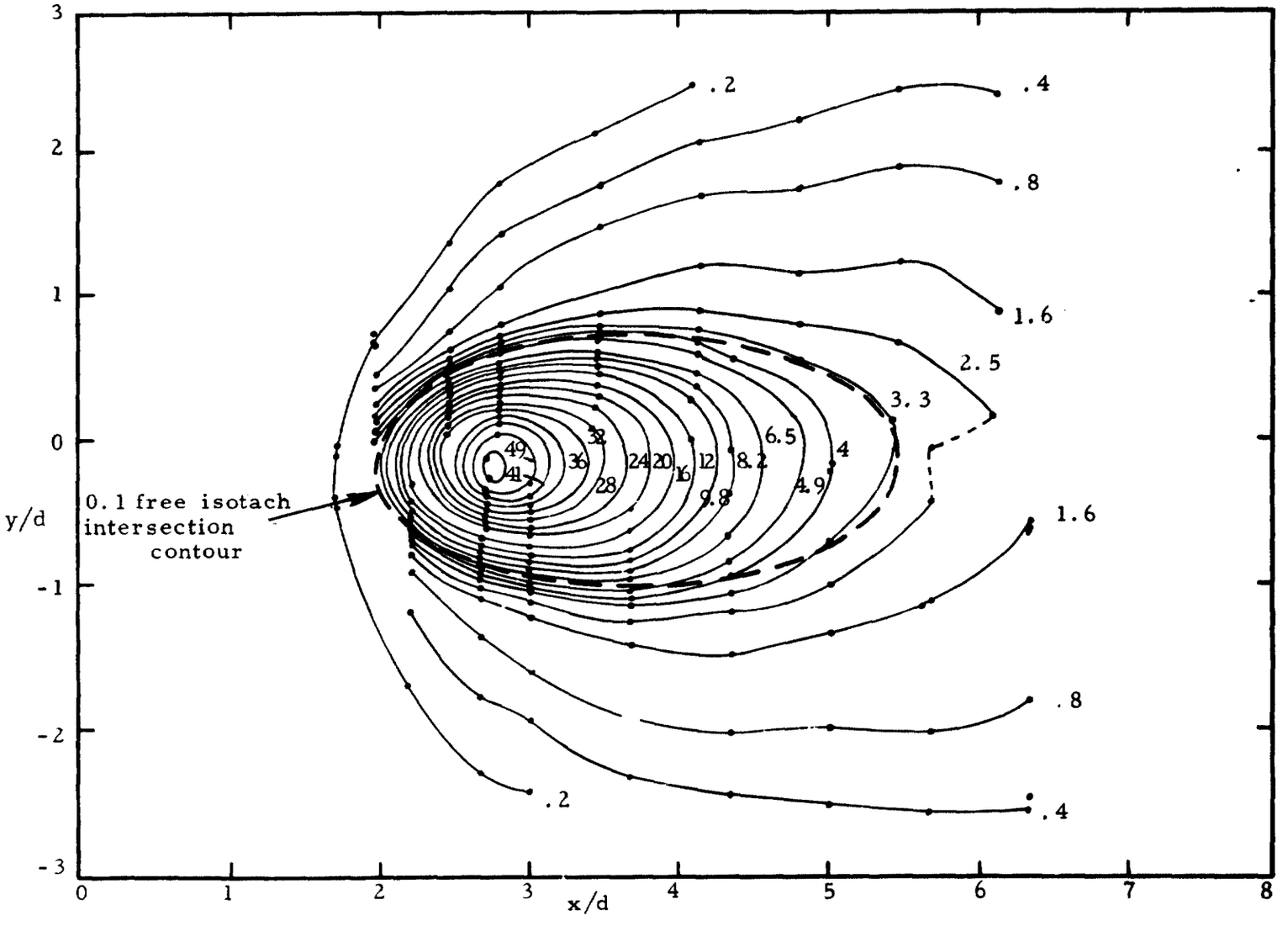
3
2
1
0
-1
-2
-3
0
1
2
3
4
5
6
7
8
x/d
y/d
.2
.4
.8
1.6
2.5
3.3
6.5
4
4.9
9.8
8.2
12
16
20
24
28
32
36
41
49
0.1 free isotach
intersection
contour
1.6
.8
.2
.4

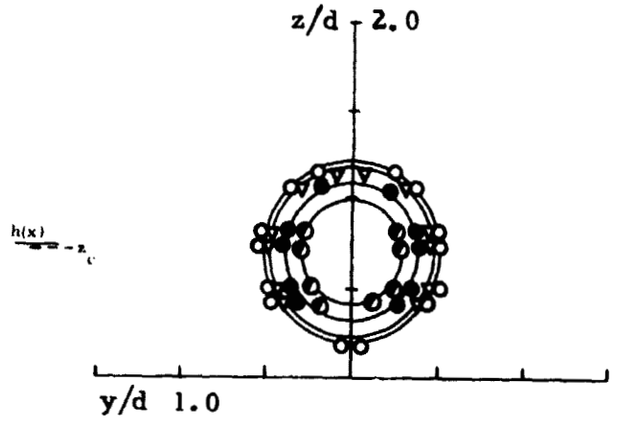

a) x/d = 0

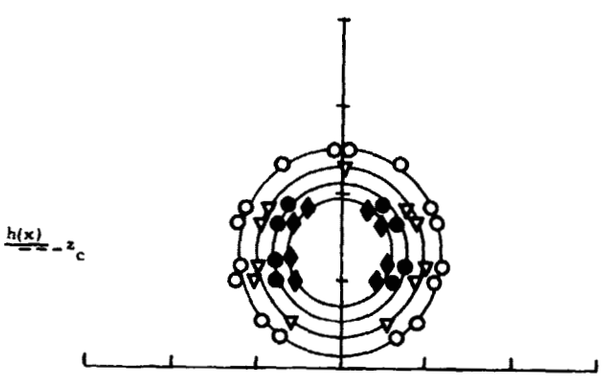

b) x/d = 1

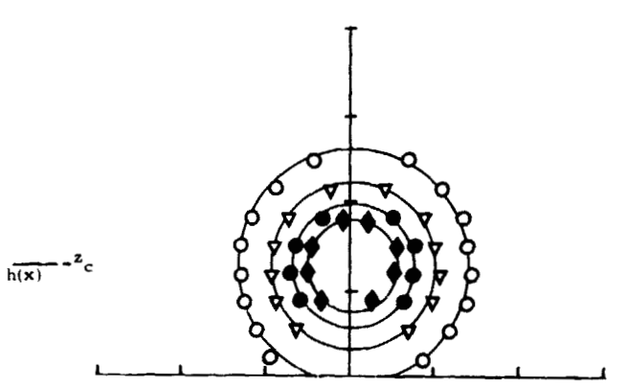

c) x/d = 2

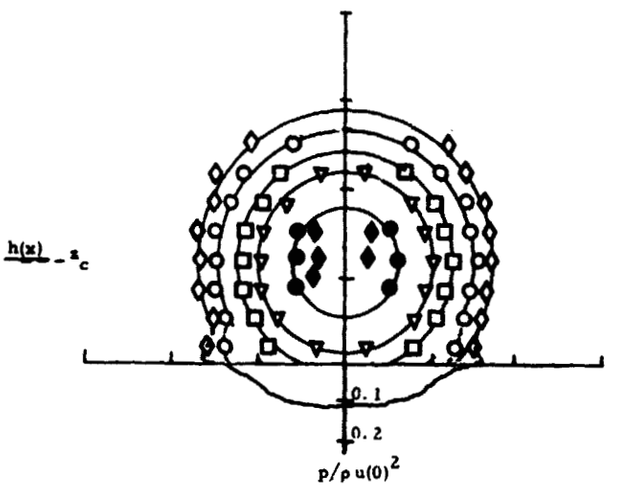

d) x/d = 3

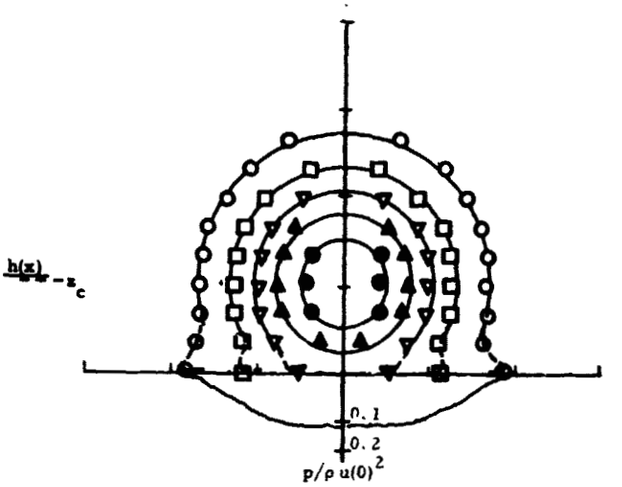

e) x/d = 4

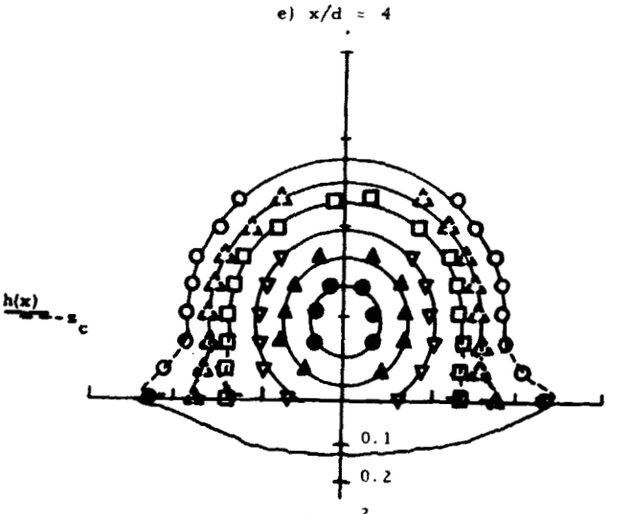

f) x/d = 5

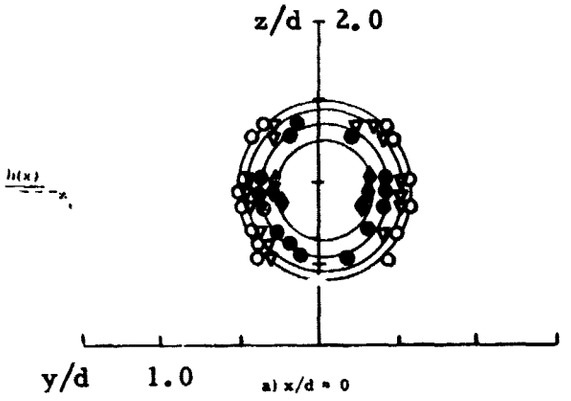

a) x/d = 0

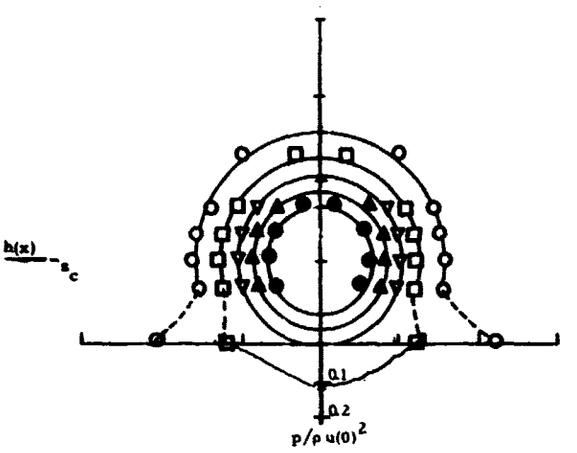

d) x/d = 3

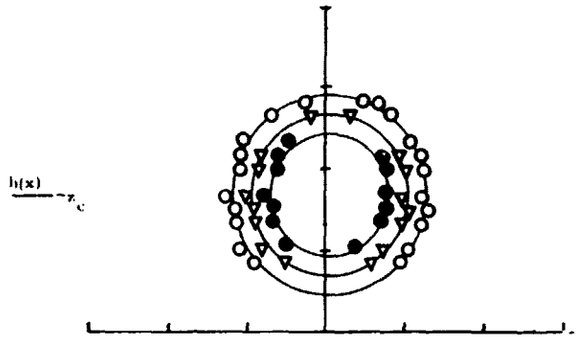

b) x/d = 1

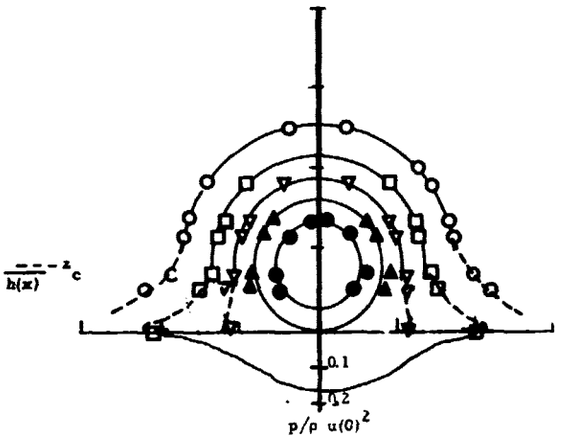

e) x/d = 4

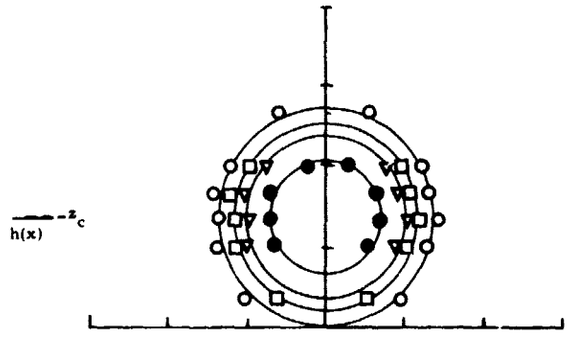

c) x/d = 2

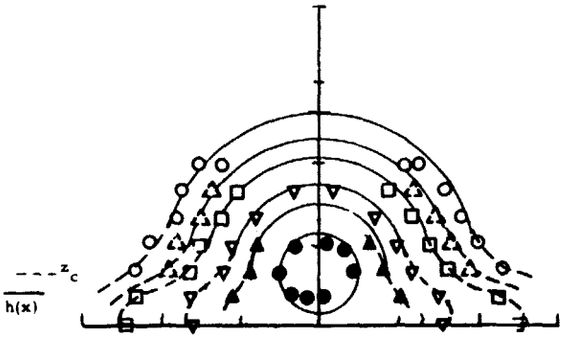

f) x/d = 5

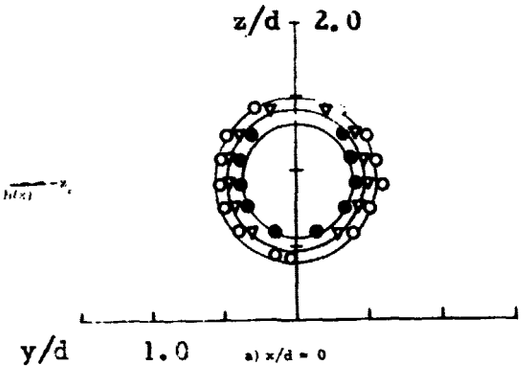

a) x/d = 0

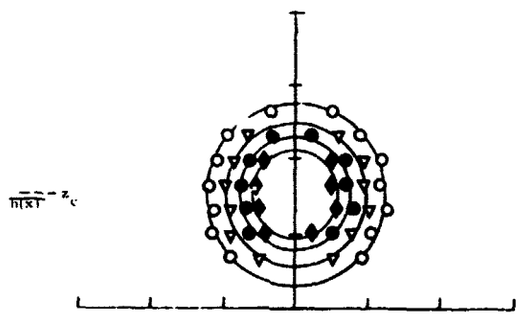

b) x/d = 1

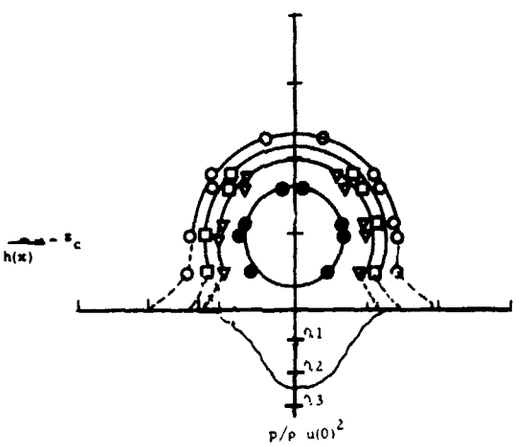

c) x/d = 2

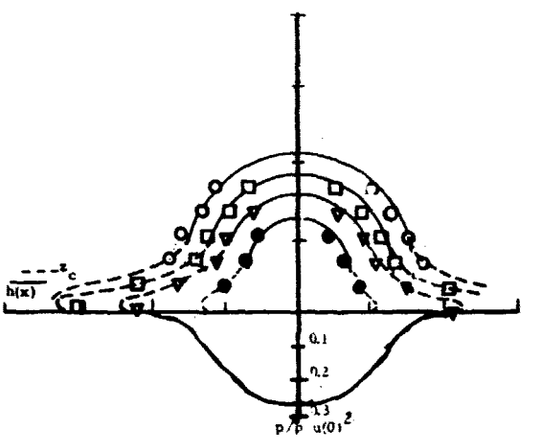

d) x/d = 3

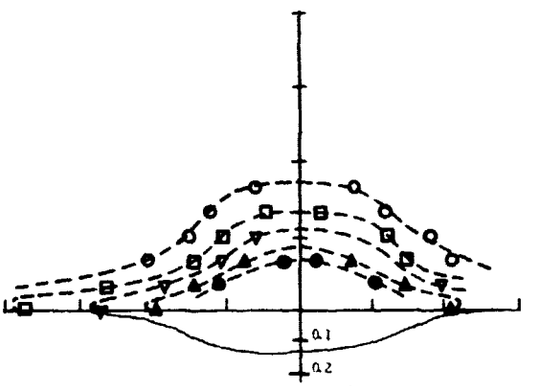

e) x/d = 4

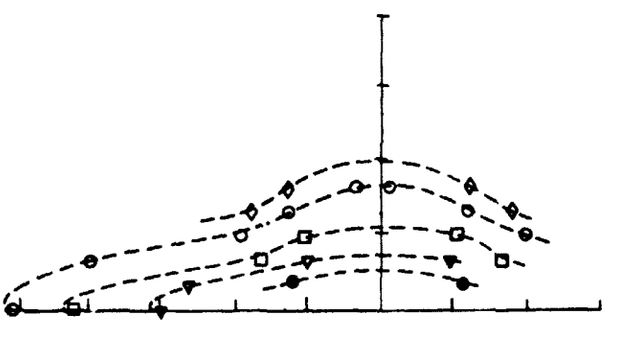

f) x/d = 5

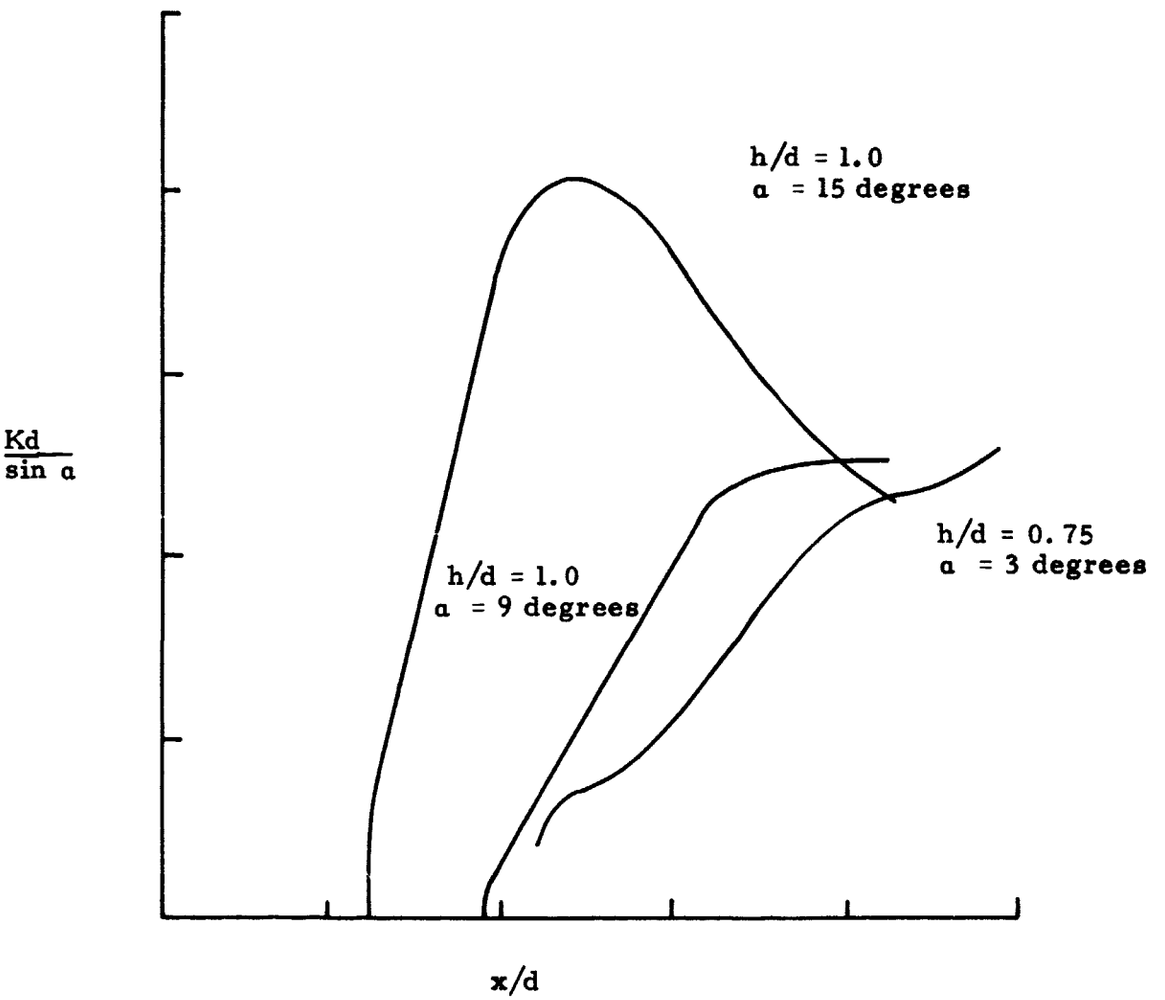
h/d = 1.0
α = 15 degrees
h/d = 1.0
α = 9 degrees
h/d = 0.75
α = 3 degrees
Kd / sin α
x/d

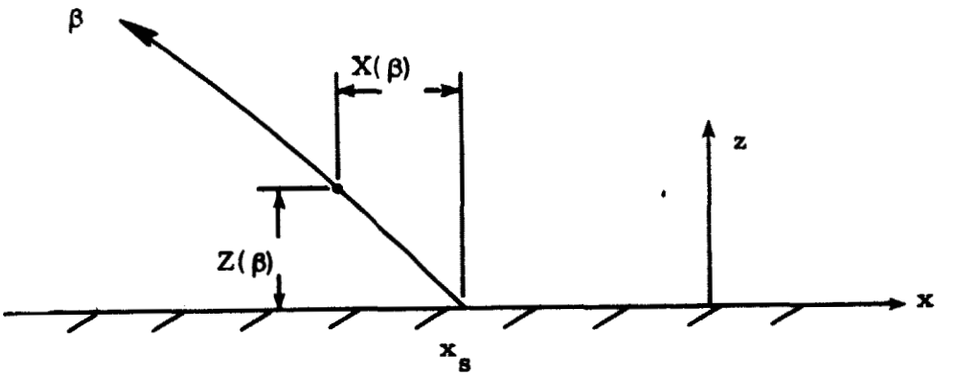

a) Definition of symbols used in the stagnation point analysis.

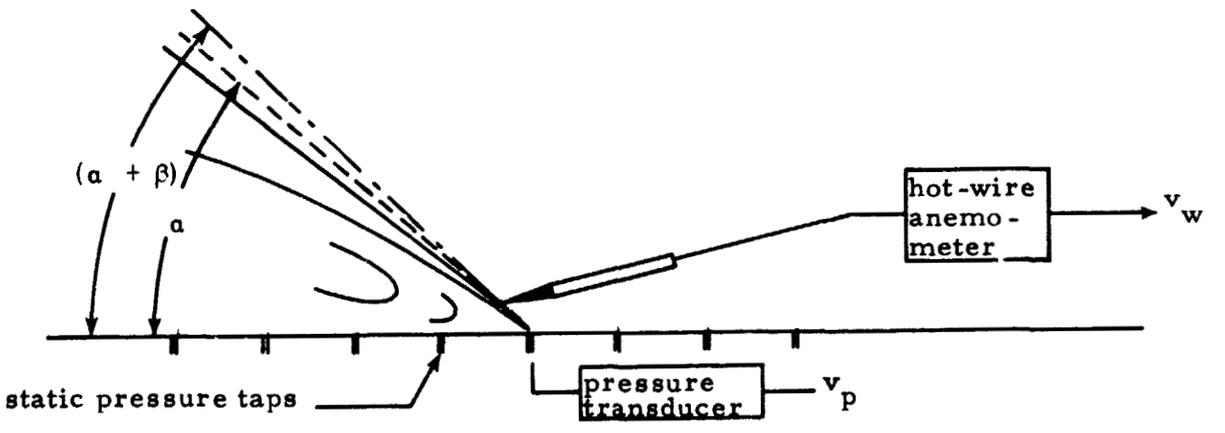

b) Experimental technique to identify the stagnation point.

$$v_p(x,0,0) = \frac{2}{\rho}[p(x,0,0) - p_{atm}]^{1/2}$$

$v_w(x,0,0)$ = v measured at z/d = 0.0328 and shifted by $\Delta x = \Delta z/\tan(\alpha + \beta)$ (β = spread angle of 0.1 free isotach)

Solid curve shows additional shift to indicate the stagnation point.

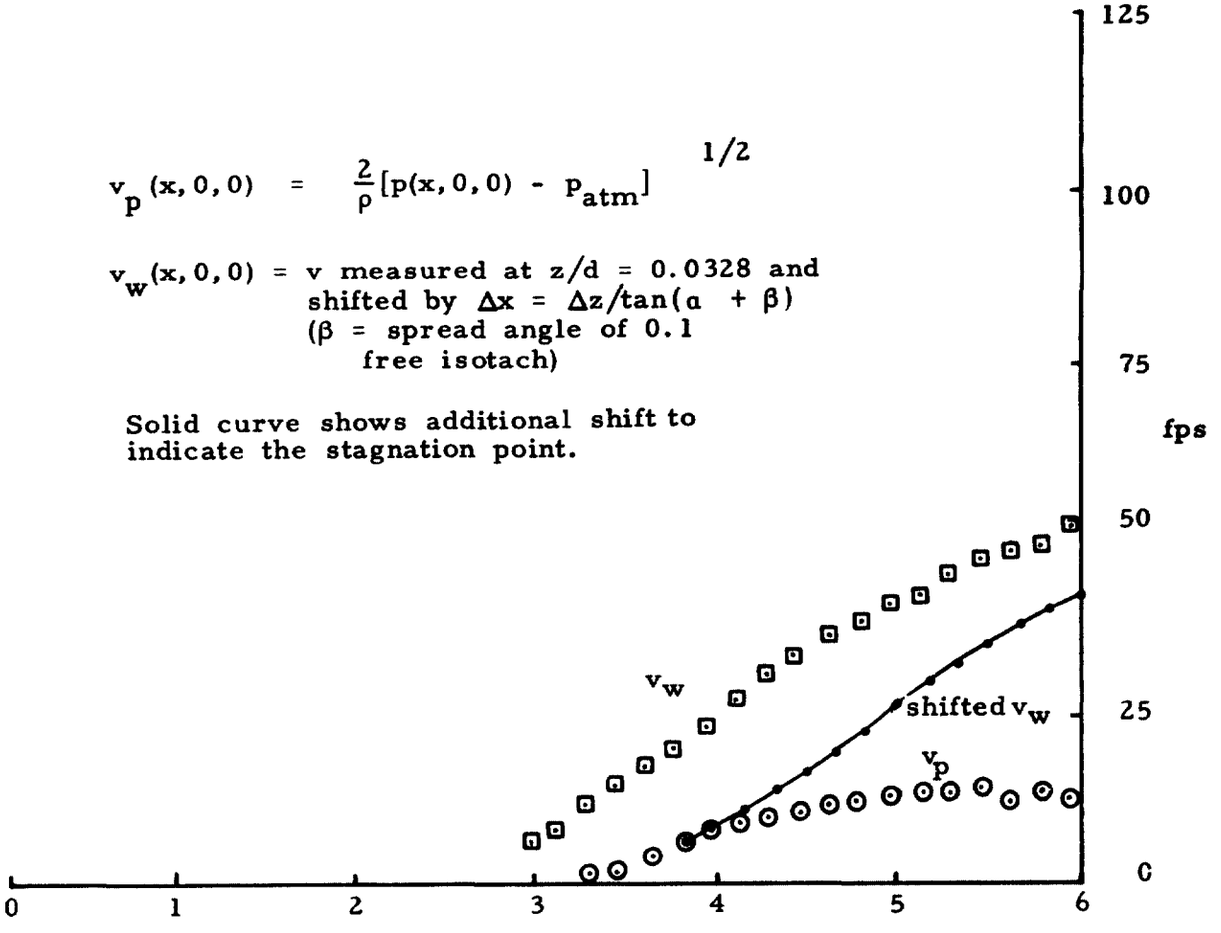

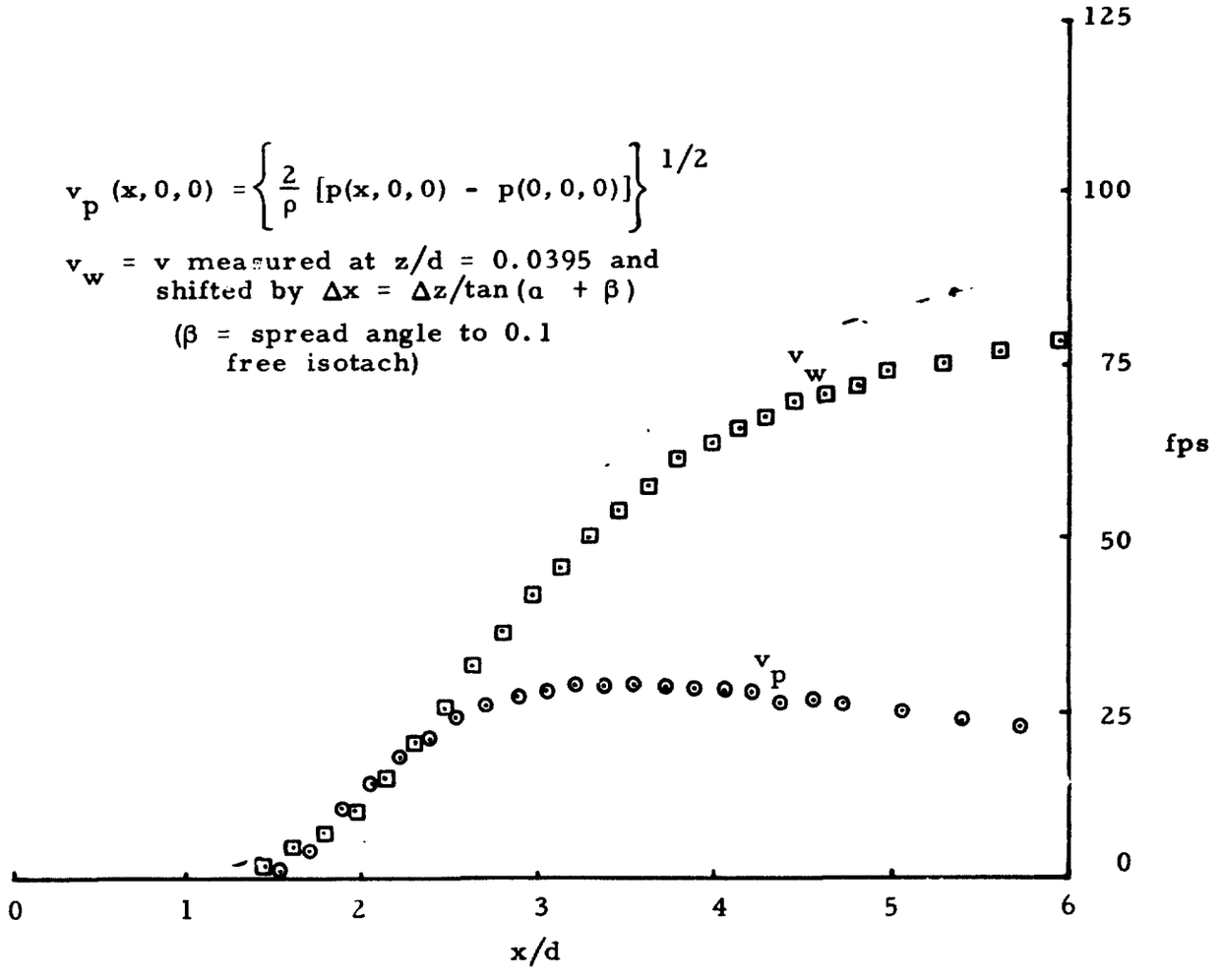
$v_p(x,0,0) = \left\{\frac{2}{\rho}[p(x,0,0) - p(0,0,0)]\right\}^{1/2}$
v_w = v measured at z/d = 0.0395 and shifted by $\Delta x = \Delta z/\tan(\alpha + \beta)$
(β = spread angle to 0.1 free isotach)
v_w
v_p
125
100
75
50
25
0
fps
0
1
2
3
4
5
6
x/d

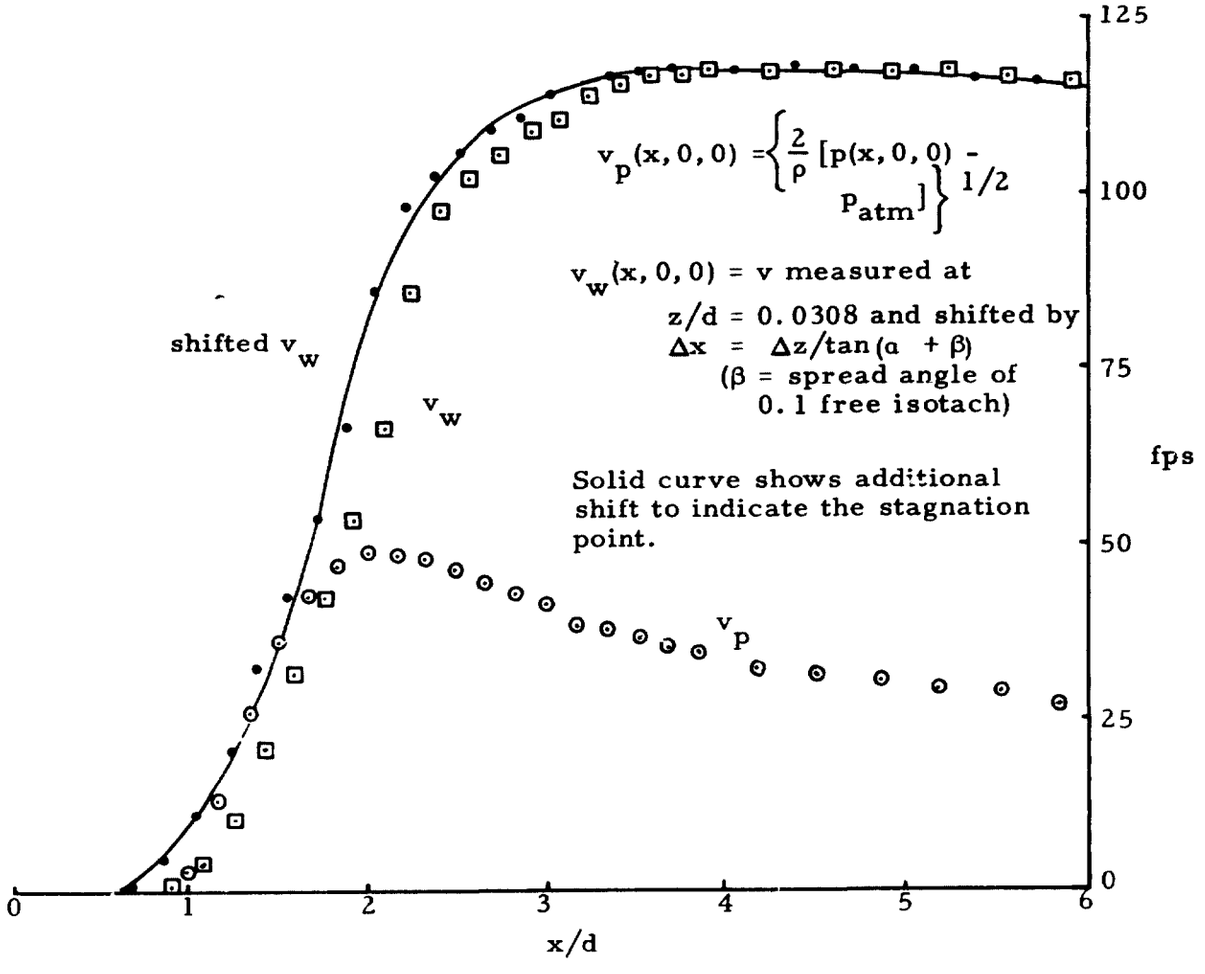
125
100
75
50
25
0
fps
0
1
2
3
4
5
6
x/d
$v_p(x,0,0) = \left\{\frac{2}{\rho}[p(x,0,0) - p_{atm}]\right\}^{1/2}$
$v_w(x,0,0)$ = v measured at z/d = 0.0308 and shifted by $\Delta x = \Delta z/\tan(\alpha + \beta)$ (β = spread angle of 0.1 free isotach)
Solid curve shows additional shift to indicate the stagnation point.
shifted v_w
v_w
v_p